Unraveling the CO2 reaction mechanism in bio-based amino-acid ionic liquids by operando ATR-IR spectroscopy

(Article begins on next page)

14 October 2023

UNIVERSITÀ DEGLI STUDI DI TORINO

Unraveling the CO_2 reaction mechanism in bio-bases amino-acid ionic liquids by operando ATR-IR spectroscopy

by

G. Latinia, M. Signorile, V. Crocellà, S. Bocchini, C. F. Pirri, S. Bordiga

Catalysis Today, in press

DOI: 10.1016/j.cattod.2018.12.050

Unraveling the CO_2 reaction mechanism in bio-based amino-acid ionic liquids by operando ATR-IR spectroscopy

G. Latini[a,b], M. Signorile[c], V. Crocellà[c*], S. Bocchini[b], C. F. Pirri[a,b], S. Bordiga[c]

[a] *Department of Applied Science and Technology, Politecnico di Torino, Corso Duca degli Abruzzi, 24, 10129, Torino, Italy.*
[b] *Centre for Sustainable Future Technologies CSFT@PoliTo Istituto Italiano di Tecnologia, Via Livorno, 60, 10144, Torino, Italy.*
[c] *Department of Chemistry, NIS and INSTM Reference Centre, Università di Torino, Via G. Quarello 15, 10135 and Via P. Giuria 7, 10125 Torino, Italy.*
*corresponding author (valentina.crocella@unito.it)

Abstract

Tackling global warming through the reduction of greenhouse gases is a key challenge mankind is called to face in the close future. Carbon dioxide is one of the main causes of such temperature increase, thus avoiding its release in the atmosphere through capture and/or utilization strategies is a valuable tool to limit greenhouse effect. Presently, the applied technology for sequestrating CO_2 relies on its reaction with amines in aqueous solutions, giving rise to the formation of carbamates and carbonates. However, due to the energy intensive release step, toxicity and corrosiveness, amine scrubbing could not represent a long-term solution in CO_2 capture. Ionic liquids (ILs), organic salts in the liquid state near room temperature, are a class of emerging materials with a great potential towards CO_2 capture. Recently the combination of the choline cation with amino acids based anions gave rise to a wide set of bio-inspired ILs with low toxicity, that, due to the presence of amino groups in the amino acid moiety, are optimal candidates for CO_2 capture. In the present work, two choline-amino acids ILs were synthesized, containing glycine and proline, according to an innovative procedure, overcoming some drawbacks proper of the classical methods. A throughout IR operando study of the CO_2 absorption process in these amino acids based ILs was performed. Even though elementary reactions are the same for all the investigated systems, different absorption pathways were recognized depending on the amino acid based anion. The reversibility of the absorption process differs between the two systems as well, further remarking the role played by the selected amino acid in the overall absorption performances. Such fundamental information, still missing in the literature, will contribute to rationally develop choline-amino acids ILs with optimal CO_2 absorption/activation properties.

Keywords: ionic liquids, amino acids, CO_2 capture, operando ATR-IR spectroscopy, carbamic acid, ammonium-carbamate.

1. Introduction

Since the mid-20th century, the mean temperature of the Earth started rising. [1] The human influence on this event is not negligible, in fact the emission of gases such carbon dioxide (CO_2), methane (CH_4), nitrous oxides (NO_x) and chlorofluorocarbon (CFC), due to the progressive industrialization, contributes to enhance the so-called "greenhouse effect", leading to the global warming. CO_2 is the most responsible for greenhouse effect, because of its disproportional abundance in the atmosphere. [2] Its concentration raised due to human activities,[3] and, recently, overstepped the concentration of 400 ppm. [4] The primary sources of CO_2 emissions are the combustion of fossil fuels, which is still widely applied in transportation, electric power generation and in several energy-intensive industrial processes. Other sources include specific manufactures, where CO_2 is a by-product (*e.g.* concrete production) and intensive livestock farming.

CO_2 removal from these gaseous emissions, its storage or its conversion in other chemicals are some of the possible strategies to tackle the climate change: these technologies should be developed with a minimum of additional energy consumption. [5] Furthermore, capture/conversion systems with low or nil toxicity, chemical stability and low cost are highly desirable.

Many technologies are available for CO_2 separation taking advantage of different physico-chemical mechanisms, *e.g.* based on adsorption, absorption, membrane separation or cryogenic separation. [5] Currently, the most exploited method relies on ammine scrubbing: [6,7] aqueous solutions of alkylammines chemically react with the CO_2 forming ammonium-carbamate (two amines per one CO_2 molecule, 2:1 mechanism) and ammonium-carbonate species (tertiary amine and water involved), as shown Scheme 1. [8–10]
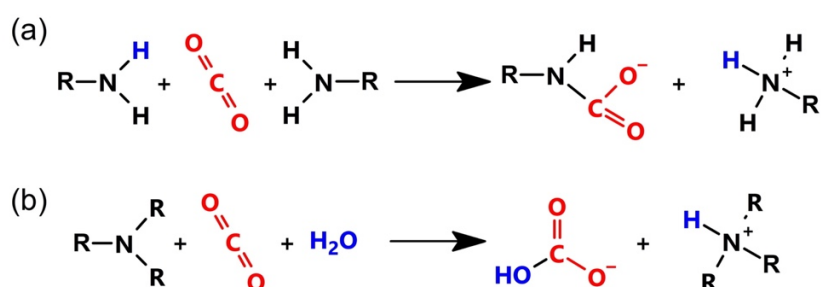
Scheme 1 Chemical reaction between alkylamines and CO_2: (a) ammonium-carbamate formation; (b) carbonate formation.

Unfortunately, amine scrubbing has several drawbacks such as high-energy costs for regeneration (since the working solvent, *i.e.* water, must be evaporated in order to release CO_2), solvent loss, corrosion and toxicity. Furthermore, once the CO_2 is captured, it has to be managed in some way: beside the bare storage, a possible strategy is to convert it into useful chemicals, thus considering CO_2 as an environmental friendly carbon feedstock rather than a waste to be disposed. However, only few processes presently reached industrial scale. [11–13] The main reason is the poor reactivity of carbon dioxide, due to the absence of dipole moment and to the high oxidation state of the carbon atom, thus

hampering the development of industrial-scale conversion processes. The most promising paths for CO_2 utilization rely on its catalytic activation: since the CO_2 is slightly acidic, basic catalysts have been widely studied. [14] Several thermo-, electro- and photo-catalytic processes have been proposed, such as the synthesis of carbonates (both inorganic and organic), the reduction to simple organic molecules (*e.g.* methanol, formic acid, etc.) and the dry reforming with methane to syngas. [12,13,15,16]

Ionic liquids (ILs), commonly defined as materials constituted by cations and anions which melt at or below 100°C [17,18] , are an emerging class of material in the field of CO_2 capture and conversion. [19–22] On the capture side, ILs can overcome some critical issues related to the use of amines aqueous solutions, since they are non-volatile, non-corrosive and highly stable. [23–27] Thanks to the variety of cations and anions which can be combined to form ILs, these compounds can absorb CO_2 on the basis of several different physico-chemical mechanisms. In the simplest case, *i.e.* when the IL does not contain CO_2-affine functional groups, only physical absorption occurs at high pressure. However, CO_2 absorption capacity can be improved (thus decreasing the working pressure) by including functionalities, such as amine groups in the cation and/or anion, [28] which increases the CO_2 absorption capacity per given amount of IL. Similarly to alkylamines solution, amine-based ILs [29] and amino-tethered ILs [28] react with CO_2 fixing it as carbamate, considered an activated form of carbon dioxide, [30,31] with a 2:1 mechanism. Unfortunately, during the CO_2 absorption process, the ILs viscosity increases, [32] thus reducing their gas-diffusion properties (*i.e.* limiting the absorption processes itself). As a possible solution, the dilution of ILs in proper solvents can boost their absorptive capacity, according to improved transport properties and possibly to synergic IL-solvent effects. [21,22] ILs are generally referred to as "green solvents", however, the most common cations (*e.g.* imidazolium and pyridinium) and anions (often fluorine based) do not show good biodegradability and biocompatibility. [33,34] Ions derived from metabolic molecules are possible environmental-friendly alternatives, *e.g.* choline (a proved non-toxic and biocompatible cation)[35–37] and amino acids (AAs, renewable, biodegradable, biocompatible and naturally-abundant anions). Since every AA contains amine functionalities, AA based ILs (AAILs) are in principle optimal candidates for CO_2 absorption. [38] As an example, the recent study by Gurkan et al. proved that trihexyl(tetradecyl)phosphonium prolinate, [P66614][Pro], and methioninate [P66614][Met] can achieve the equimolar absorption at a pressure of 2 bar. [39]

Despite the chemical variability offered by AAs (*i.e.* the variety of anions and their functional groups) and the encouraging properties of choline-based AAILs (including their biodegradability and potential biocompatibility), nowadays few studies have been conducted on these innovative materials. [40–47] A first limitation to their employment could be represented by the presently applied synthetic methods. [40,43,44] Even if yields higher than 90% are obtained, all these routes rely on the AAs acid-base reaction with the choline hydroxide, a strong base indeed corrosive, difficult to handle (it easily reacts with atmospheric CO_2) and quite costly. Accordingly, few examples are available concerning the interaction of Choline-AAILs with CO_2: to the best of our knowledge, only two works report about the CO_2 absorption in these materials. Zou and co-workers tested choline prolinate, [Cho][Pro], as such and diluted in polyethylene glycol 200 (PEG-200), measuring

a 0.6 CO_2-IL molar ratio for absorption at 1.1 bar. [41] Lu et al. measured the CO_2 solubility in different aqueous solution of choline glycinate, alaninate and prolinate up to 15 bar. They reported CO_2-IL molar ratio up to 2 and the hydration of carbamate to bicarbonate, due to the higher pressure employed and as a consequence of using water as solvent. [45] Moreover, all the aforementioned studies proposed minimal sets of characterization data beside the assessment of the absorption performances, thereby direct evidences about the CO_2 absorption mechanism in these Choline-AAILs are still missing. In this regard, a spectroscopic operando approach is in principle extremely valuable, since it allows to infer the CO_2-IL interaction mechanism on the basis of spectroscopic data, simultaneously monitoring the CO_2 concentration in the gas stream.

In the present work, an innovative method for synthesizing Choline-AAILs by overcoming the limitations of traditional routes is reported for the first time. This method makes use of choline chloride (a cheap and easy to handle salt) as choline cation source, avoiding the employment of the corrosive and costly choline hydroxide. Two different choline based AAILs (exploiting glycine and proline as anions) were synthesized and their interaction with a synthetic flue gas (20%v/v CO_2) at RT and atmospheric pressure was studied by means of operando infrared spectroscopy: the ILs sorbent phase and the composition of the gaseous stream were simultaneously monitored. Due to the need of characterizing a liquid phase upon interaction with a gas stream, a dedicated setup has been designed and implemented. For the first time, important mechanistic insights about the CO_2 reaction with choline-based AAILs is documented, showing the formation and the (possible) reversibility of ammonium-carbamate and carbamic acid species as a function of the CO_2 loading.


2. Material and methods

2.1 Synthesis of [Cho][Gly] and [Cho][Pro]

In a 250 ml flask, glycine (37.8 g, supplied by Merck, purity ≥99%) and an excess of potassium hydroxide (30.9 g, Carlo Erba, purity ≥85%) are mixed at RT in ethanol (200ml, supplied by Merck, purity ≥99.8%) under stirring. The potassium salt of the glycine is formed, the suspension turned white while the excess of potassium salt of the glycine precipitates. Once the potassium hydroxide pellets dissolved completely (c.ca 2 h), the choline chloride (69.8 g, supplied by Alfa Aesar, purity ≥98%) was added. The mixture was left under stirring for 4 h. The potassium salt of glycine dissolves and potassium chloride precipitated as white powder leaving choline glycinate in solution upon the exchange of K^+ by choline cations. The potassium chloride crystals were separated by centrifugation, and then ethanol and water produced during the reaction were removed using a rotary evaporator. The so obtained IL (hereafter referred to as [Cho][Gly]), was preliminary checked by means of ATR-IR spectroscopy and, then, outgassed under dynamic vacuum at 30°C overnight to totally remove the possible residual ethanol and water, prior the *operando* experiments. The synthesis of the other IL. Choline prolinate (termed as [Cho][Pro]), follows the same procedure, but using L-proline (45 g, supplied by Merck, purity ≥99%) instead of glycine. The reactions describing the whole synthetic process are

summarized in Scheme 2. The successful formation of the two ILs ([Cho][Gly] and [Cho][Pro]) has been also confirmed by ^{1}H-NMR measurements and the KCl content was evaluated by TG and XPS analyses. For the sake of brevity, these data are reported in the Sections S1, S2 and S3 of the Supplementary Material.

2.2 ILs solutions with dimethyl sulfoxide (DMSO)

[Cho][Gly] and [Cho][Pro] were diluted in dimethyl sulfoxide (DMSO, supplied by Merck, purity ≥99%) in order to decrease their viscosity. DMSO was chosen because it is completely miscible with the ILs considered in this study, it inhibits carbonates formation (DMSO is an aprotic but exhibits properties similar to water), it is non-toxic and it has a high boiling point. DMSO allows the use of pressure/temperature switching to recover CO_2 without solvent evaporation/condensation, thus reducing the energy required for CO_2 desorption in comparison with aqueous amines systems. Dilutions in DMSO were performed to reach a 16%wt/wt concentration. A more concentrated solution of [Cho][Gly] (50%wt/wt) was prepared as well. The ILs dilution was performed just prior the beginning of the absorption experiment, thus reducing the extent of CO_2 spuriously captured from the atmosphere.
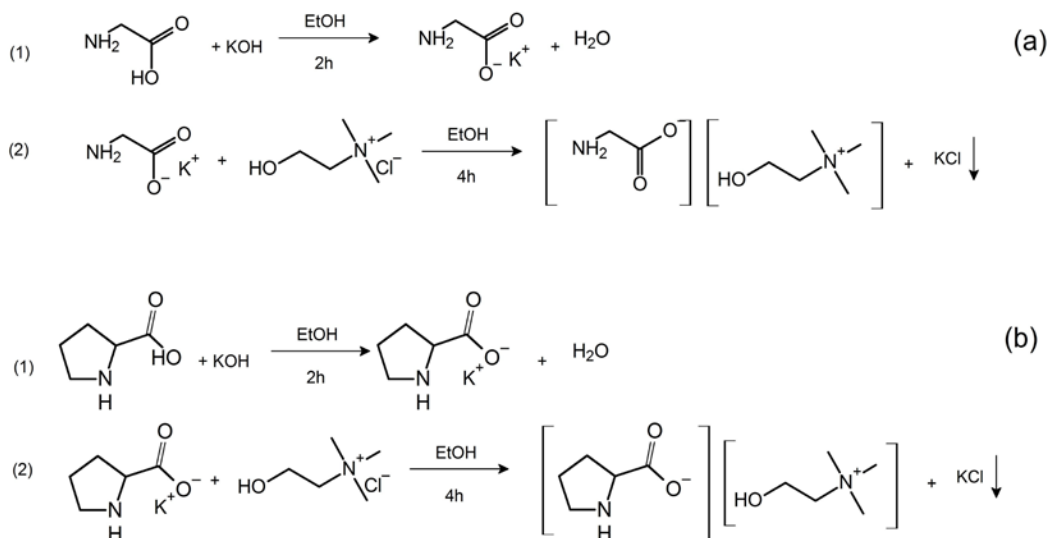
Scheme 2 Synthesis pathways of [Cho][Gly] (a) and [Cho][Pro] (b)

2.3 CO_2 absorption quantification

The CO_2 absorption quantification of [Cho][Gly] and [Cho][Pro] were tested using a gravimetric method. In a reactor (volume ~4.5 ml), ~3ml of IL-DMSO solution was poured and purged with N_2 (50 ml/min) for 10 minutes and the weight of the solution was acquired. Then, CO_2 (50 ml/min) was bubbled in the solution until the weight ceased to increase. During the whole procedure, the IL-DMSO solution was kept under stirring. The absorbed CO_2 was quantified by mass difference before and after CO_2 bubbling, taking into account the headspace of the vessel. Two physical quantities were calculated: the absorption capacity, defined as the weight ratio between the absorbed CO_2 and the liquid solution,

and the molar efficiency, defined as molar ratio between the absorbed CO_2 and the IL present in the solution. Different IL dilutions in DMSO were tested: 50, 33.3, 20, 16 %wt/wt.

A custom reactor made by HEL Group was employed to investigate the effect of the temperature on the absorbed CO_2 and on the release process. For the sake of brevity, the schematics are reported in Section S4 of the Supplementary Material. The absorption experiments for the quantification of the absorbed CO_2 were performed at three temperatures: 25, 30 and 40°C on a 16%wt/wt [Cho][Pro]-DMSO solution. In a typical experiment, during the initial temperature stabilization step, the DMSO-IL solution (~5 ml) was purged with N_2 (40 ml/min). Then, the gas composition was changed to CO_2/N_2 20:80 (40 ml/min) until saturation of the solution. At the end of the absorption step, the gas was switched back to pure N_2 (40 ml/min) and the temperature was kept constant. After 10 minutes, the reactor was heated up (ramp 5°C/min) to 80°C, keeping this temperature until CO_2 becomes undetectable.

2.4 FT-IR spectroscopic measurements.

The characterization of the pure ILs and the study of CO_2 interaction have been performed by means of two different FT-IR spectrophotometers (termed as IR1 and IR2), coupled in the case of the use of the experimental setup for simultaneous liquid and gas IR monitoring described in the following section.

IR1. Bruker Vertex 70 spectrophotometer equipped with a Mercury-Cadmium-Telluride (MCT) cryodetector and coupled with an Axiom-Hellma TNL 130H multiple-reflections attenuated total reflectance (ATR) cell specifically designed for liquid samples. The cell is operated through an AMTIR-1 optical element. This spectroscopic setup was employed to acquire *in situ* the ATR spectra of the IL-DMSO mixture (as such and in interaction with CO_2). A single-reflection Platinum ATR accessory provided by Bruker, equipped with a diamond crystal, was instead exploited for the basic post-synthetic characterization of the pure ILs and their precursors. All the spectra were recorded at a resolution of 2 cm^{-1}, by accumulating 32 scans in the 4000–600 cm^{-1} spectral range.

IR2. Jasco FT/IR-6100 spectrophotometer equipped with a DTGS detector, allowing collecting gas-phase spectra in transmission mode by means of a home-made gas cell with an optical path of 19 cm to quantify the CO_2 concentration. Each spectrum was recorded at a resolution of with 2 cm^{-1}, by accumulating 32 scans within the 4000–600 cm^{-1} spectral range. The CO_2 concentration monitoring was obtained *via* area integration of the CO_2 first overtone stretching vibrational mode in the 3400-3800 cm^{-1} range.

The whole analytical apparatus relies on the two FT-IR spectrophotometers described above: the IR1 (working in ATR mode, devoted to the liquid phase characterization) and the IR2 (working in transmission mode, adopted to monitor the gas phase effluents downstream the ATR cell). Further details about the gas-liquid supplying system are given hereafter. Aiming to perform gas absorption into a bulk liquid phase, a custom setup has been designed, according to the schematics reported in Figure 1. This setup is constituted of two separated circuits: i) a closed loop circuit intended to continuously feed the ATR cell

with the liquid phase; and ii) an open gas circuit, devoted to flow a desired gas mixture through the liquid phase within a dedicated mixing chamber.

Initially, 42 ml of IL solution in DMSO 16%wt/wt was poured in the mixing chamber. Then, the solution was circulated through the closed-loop liquid circuit by means of a peristaltic pump: during this preliminary stage, 200 ml/min of dry N_2 were bubbled through the IL solution inside the mixing chamber, employing the open gas circuit, to purge the gas system from any residual CO_2. After 10 min of purging, the gas flow was directed through a bypass line (*i.e.* avoiding its mixing with the IL solution) and the gas phase composition was changed to 20 vol% CO_2 in N_2 (200 ml/min total flow), in order to simulate a typical flue gas. [48] The gas flow rate for each pure gas was controlled through a Delta Smart II digital mass flow controller (MFC), supplied by Brooks Instrument. The bypass line allowed the assessment of the initial composition of the model flue gas by IR2: to this purpose, a 5 min baseline was collected with a 30 s/spectrum sampling rate. Then, the gas flow was bubbled through the IL solution inside the mixing chamber, thus allowing CO_2 from the flue gas to be adsorbed by the IL solution. Meanwhile, the liquid phase was synchronously monitored by IR1. The synthetic flue gas was bubbled until saturation occurred, *i.e.* when the concentration of monitored CO_2 has returned back to the baseline level. After that, the gas stream was switched to pure N_2 and directed to IR2 in order to acquire a N_2 baseline (5 min stream, 10 IR spectra). At this moment, the N_2 flow was bubbled inside the liquid in the mixing chamber until no more CO_2 was measured by IR2. The above described procedure was performed once in the presence of both [Cho][Gly] and [Cho][Pro]. [Cho][Pro] underwent an additional shorter absorption cycle.
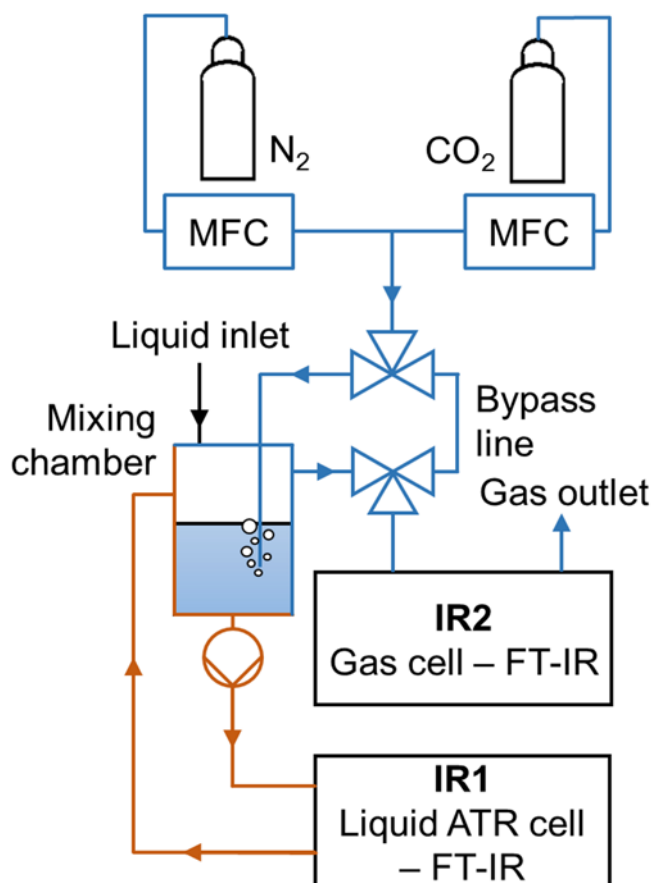
Figure 1 Schematic of the experimental setup for simultaneous liquid and gas IR monitoring. The liquid circuit is highlighted in orange, the gas one in blue.


3. Results and discussion

3.1 Infrared characterization of pure ILs

Pure [Cho][Gly] and [Cho][Pro] have been preliminary characterized by means of ATR-IR spectroscopy, aiming to prove the successful synthesis of the IL and, at the same time, to unequivocally identify the main spectral features of the amino acid moieties in the pure ILs that will be directly involved in the CO_2 absorption process.

The ATR-IR spectra of [Cho][Gly] and [Cho][Pro] (both collected immediately after the solvent removal at the rotary evaporator), together with ones of their precursors, are depicted in the 1800-1100 cm^{-1} spectral region in Figure 2a and 2b respectively. The insets report the spectra in the higher wavenumber region (3650-2550 cm^{-1}). Comparing the spectra of the precursors (the solid amino acid and the choline chloride) with those of the final ILs, it is evident that both of them are not a bare mixture of the reagents. The spectra of the solid crystalline amino acids, that usually exist in zwitterionic form (hereafter z-, see chemical structures (i) and (iii) in Figure 2), both exhibit the spectral features of the protonated amino group and of the carboxylate anion. Indeed, the bands at 1573 and 1389 cm^{-1} and at 1611 and 1405 cm^{-1} (see the blue spectra in Figure 2a and 2b) can be ascribed to the asymmetric and symmetric stretching vibrational modes (ν_{OCO-}) of the carboxylate moieties in z-glycine and z-proline respectively. [49–51] The existence of the amino groups in protonated form are testified by the presence of the bands at 3100, 1627 and 1495 cm^{-1} generated by the asymmetric stretching and the asymmetric and symmetric bending vibrational modes of the NH_3^+ moiety of z-glycine (blue spectrum in figure 2a) and of the signals located at 3050 and 1550 cm^{-1} due to the asymmetric stretching vibration and the in-plane bending mode of NH_2^+ group of z-proline form (blue spectrum in figure 2b). [49–51] Still, the intense signal present in solid z-proline at around 1373 cm^{-1} is ascribed to the bending mode of the CH group in the heterocyclic ring.

Passing from the solid amino acids to the ILs, evident spectral changes are expected due to the fact that, thanks to the presence of the choline acting as positive counter ion (that maintains electrical neutrality in the final IL) the amino acids can be found in their alkaline form, *i.e.* with a neutral amine moiety and carboxylate anionic group (see chemical structure (ii) and (iv) in Figure 2). Therefore, the successful formation of the two ILs is proved by (see black spectra of Figure 2a and 2b) (i) the existence of the carboxylate groups fingerprints (bands at 1565 and 1390 cm^{-1} in [Cho][Gly] and at 1584 and 1370 cm^{-1} in [Cho][Pro]), (ii) the total absence of the amino groups signals in protonated form and (iii) the presence of the spectral features of neutral amine moiety. In the case of [Cho][Gly] the NH_2 stretching vibrational mode (ν_{NH2}) is well evident at 3350 cm^{-1}. The corresponding deformation vibration (δ_{NH2}), instead, is not distinguishable at around 1600 cm^{-1} due to the superimposition of the intense carboxylate asymmetric ν_{OCO-} band, that is located in the same spectral range. For what concerns [Cho][Pro], a broad signal at around 3250 cm^{-1}, generated by the NH stretching vibration (ν_{NH}) of the neutral amine moiety inserted in the

heterocyclic ring, is observable, together with the absence of the NH_2^+ group fingerprints. Again, the NH deformation is not observable due to the superimposition of the choline vibrational modes in the same spectral region. Moreover, it is worth noting that in [Cho][Pro] the carboxylate stretching vibrations redshift of 30 cm^{-1} with respect to the solid z-proline, due (probably) to a significant interaction with the choline cation. Moreover, it is clear that the symmetric ν_{OCO^-} in [Cho][Pro] at around 1370 cm^{-1} is overlapped to the bending mode of the CH group located in the heterocyclic ring.
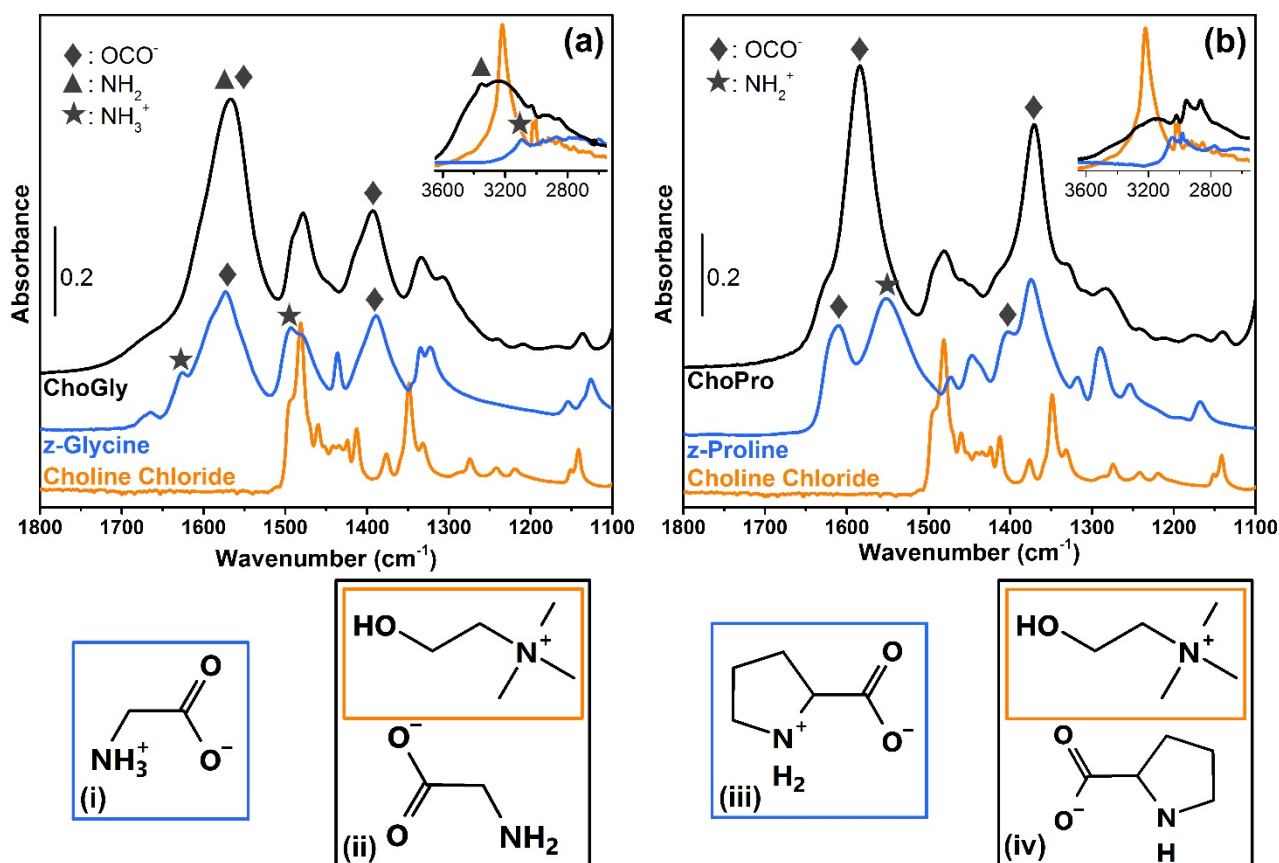
Figure 2 Section (a): ATR-IR spectrum of [Cho][Gly] ionic liquid (black curve), compared to the reference spectra of choline chloride (orange curve) and solid z-glycine (light blue curve). Section (b): ATR-IR spectrum of [Cho][Pro] ionic liquid (black curve), compared to the reference spectra of choline chloride (orange curve) and solid z-proline (light blue curve). The two insets report the same spectra in the higher wavenumber region (3650-2550 cm^{-1}). In both sections the signals related to the main functional groups vibrational modes are labeled: carboxylate groups (diamonds), neutral amines (triangles) and protonated amine moieties (stars). Bottom: chemical structures of the amino acids in zwitterionic form (i, z-glycine and iii, z-proline) and of the final ILs (ii, [Cho][Gly] and iv, [Cho][Pro]).

The main spectral features of choline are evident in the 1500-1450 cm^{-1} region in the spectra of both ILs. Differently, the OH stretching vibrational mode of pure choline chloride,

present as a narrow peak at 3220 cm^{-1}, undergoes evident transformations in the final ILs giving rise to a broad envelope in the 3600-3100 cm^{-1} range overlapped to the signals of both not protonated amine moieties and of the small fraction of water still present in the ILs after the preliminary solvent removal by rotary evaporator. [49] These changes testify that the OH group of choline probably interacts with the amine moiety or the carboxylate group of the amino acid of a neighboring ionic couple.

The assignment of the main vibrational frequencies of z-proline and z-glycine and of their ILs from the IR spectra of Figure 2, made according to ref.[49], [50] and [51], are summarized in Table 1.

Table 1 Assignment of the main vibrational frequencies in the IR spectra of Figure 2, related to the carboxylate groups and to the amine moiety in both neutral and protonated forms present in solid z-proline and z-glycine and in their respective ILs. [a,b]

Functional Group	z-Glycine	[Cho][Gly]	z-Proline	[Cho][Pro]
Carboxylate (OCO$^-$)	1573 (ν_{as})	1565 (ν_{as})	1611 (ν_{as})	1584 (ν_{as})
	1389 (ν_{sym})	1390 (ν_{sym})	1405 (ν_{sym})	1370 (ν_{sym}) [c]
Protonated amine (NH$_3^+$ or NH$_2^+$)	3100 (ν_{as})	-	3050 (ν_{as})	-
	1627 (δ_{as})		1550 (δ)	
	1495 (δ_{sym})			
Neutral amine (NH$_2$ or NH)	3350 (ν_{as})	-	-	~3250 (ν) [e]
	~1600 (δ) [d]			

[a] Assignments made according to ref. [49], [50] and [51]
[b] All wavenumber values are in cm^{-1}. ν, stretching; δ, bending; as, asymmetric; sym, symmetric.
[c] Overlapped to the to the bending mode of the CH group of the heterocyclic ring.
[d] Overlapped to the to the asymmetric OCO$^-$ stretching mode.
[e] Overlapped to the OH stretching group of choline.

3.2 CO$_2$ absorption quantification

The absorption capacity (AC) and molar efficiency (ME) of different IL-DMSO solutions were measured and reported in Table 2. Both [Cho][Gly] and [Cho][Pro] were tested, as reported in the experimental section, using different dilutions (50, 33.3, 20, 16%wt/wt). By comparing the absorption capacities with the same dilution, [Cho][Gly] always exhibits higher absorption values than [Cho][Pro]. This fact can be explained considering the lower molecular weight of [Cho][Gly] with respect to [Cho][Pro], that leads to a higher amount of amine species per weight unit. In addition, it is worth noticing the proportionality between the IL concentration and the absorption capacity (*i.e.*, the higher IL concentration, the higher absorption capacity). By considering the ME, it is evident that all the values reported in Table 2 are higher than 0.5 mol(CO$_2$)/mol(IL), meaning that all the IL-DMSO

solutions exceed the theoretical stoichiometry of the CO_2-amine absorption, in which two amines react with one CO_2 molecule (see Scheme 1). The CO_2 excess could be absorbed in the form of carbamic acid. Nonetheless, it worth highlighting that the lower the IL concentration the higher the ME. It is possible to hypothesize that the dispersion of the absorbing molecules inside the bulk liquid affects the absorption mechanism, favoring the formation of carbamic acid or the ammonium-carbamate couple. Comparing the MEs, both the ILs show the same value at 50%wt/wt concentration, whereas at lower IL concentrations, [Cho][Gly] manifests higher MEs than [Cho][Pro].

The dilution exhibiting the higher ME (16 %wt/wt) has been chosen to be studied using the operando spectroscopic setup in order to determine the IL-CO_2 interaction and to identify the chemical species deriving from this reactivity.

Table 2 CO_2 absorption performances of [Cho][Gly] and [Cho][Pro] as a function of their concentration in DMSO.

IL concentration[a]	[Cho][Gly]		[Cho][Pro]	
	AC[b]	ME[c]	AC[b]	ME[c]
50	8.58 ± 0.18	0.70 ± 0.07	7.03 ± 0.19	0.70 ± 0.07
33.3	6.06 ± 0.16	0.74 ± 0.07	4.63 ± 0.22	0.69 ± 0.07
20	4.07 ± 0.18	0.83 ± 0.08	2.95 ± 0.17	0.73 ± 0.07
16	3.35 ± 0.15	0.86 ± 0.09	2.39 ± 0.17	0.75 ± 0.08

[a] IL concentration expressed as %wt/wt
[b] Absorption capacity, expressed as %wt(CO_2)/wt(solution)
[c] Molar efficiency, expressed as mol(CO_2)/mol(IL)

3.3 *Operando* ATR-IR study of the CO_2/choline-AAILs reaction mechanism

The absorption process of CO_2 into bulk AAILs is associated with a real chemical reactivity occurring between the CO_2 molecule itself and the amine group of the amino acid anion. In this chemical context, the ATR-IR spectroscopy is probably the elective experimental tool to study the interaction mechanism of CO_2 with the selected AAILs and to unequivocally identify the chemical species generated by this reactivity. The study has been carried out by means of the *operando* ATR-IR setup described in Section 2. As reported in the Introduction and in the Material and Methods sections, the AAILs have been studied by preparing solutions with DMSO to overcome the issues deriving from the high viscosity typical of these systems. [32]

3.3.1 CO_2 absorption in [Cho][Gly]-DMSO solution.

The first *operando* experiment was carried out on a [Cho][Gly]-DMSO (16%wt/wt) solution. According to the setup description reported in the experimental section, IR1 monitored the [Cho][Gly]-DMSO solution throughout the CO_2 absorption process, while IR2 measured the gas phase, allowing an evaluation of the CO_2 concentration over time. In the upper part of Figure 3 the ATR-IR spectra of the [Cho][Gly]-DMSO solution are displayed in the different stages of the CO_2 absorption process, in the spectral range of interest for the CO_2 chemical reactivity (1800-1100 cm^{-1}). For a better comprehension of the reactivity

mechanism, the spectra have been divided in two distinct sections (Figure 3a and 3b). The corresponding breakthrough curve, obtained by monitoring the gas phase during the absorption run by means of the IR2 spectrophotometer, is displayed in Figure 3c.
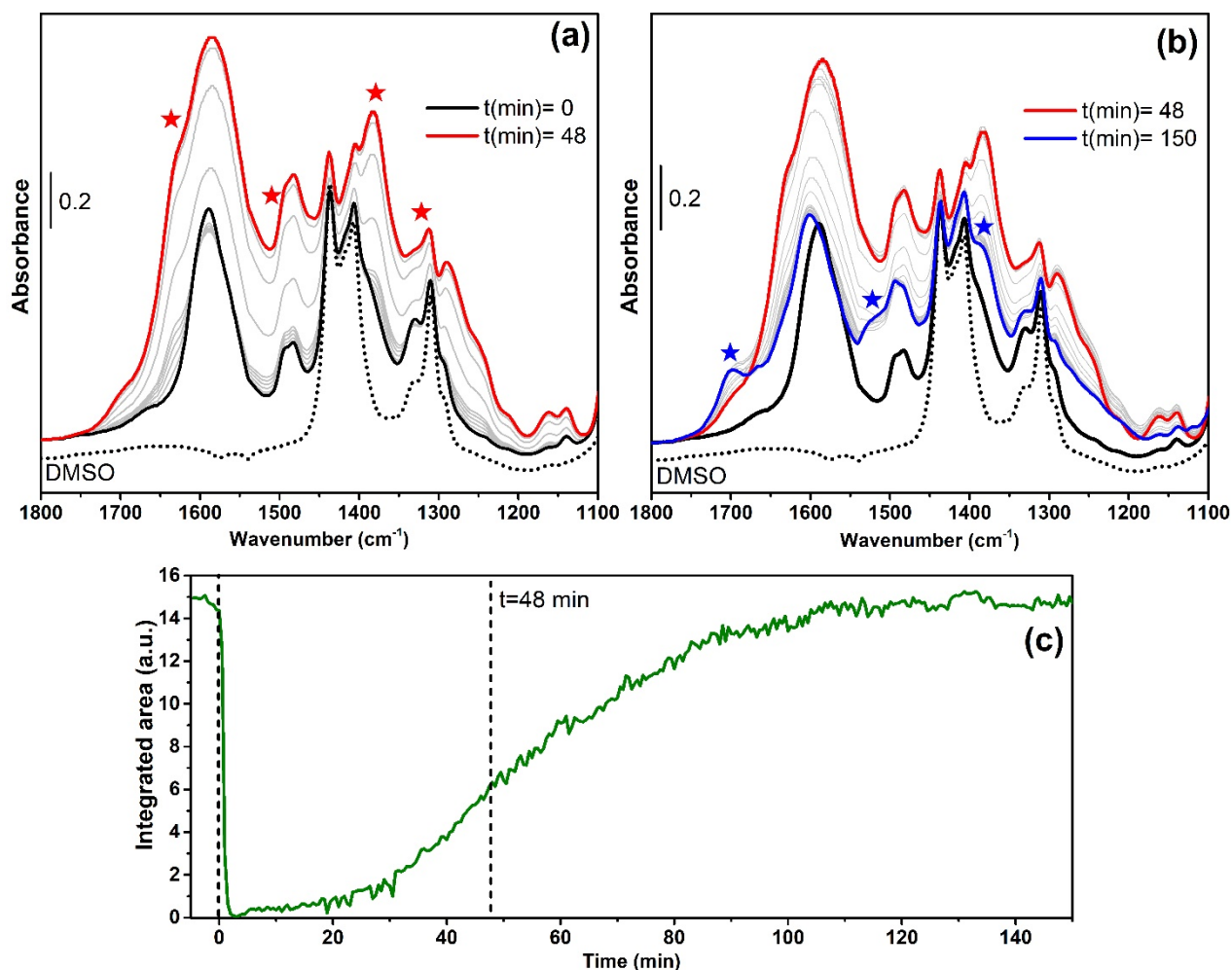
Figure 3 Section (a) and (b): time evolution of the ATR-IR spectra, in the 1800-1100 cm^{-1} spectral region, of the [Cho][Gly]-DMSO (16%wt/wt) solution in contact with a synthetic flue gas (composition: 20 vol% CO_2 in N_2). Section (a): ATR-IR spectra of pure DMSO (black dotted curve), [Cho][Gly]-DMSO solution (black curve), [Cho][Gly]-DMSO solution after 48 minutes of contact with the flue gas (red curve). Transition spectra (light grey curves) were acquired every 5 minutes. Red stars label the main spectral features appearing consequently to the CO_2 interaction. Section (b): ATR-IR spectra of [Cho][Gly]-DMSO solution (black curve), [Cho][Gly]-DMSO solution after 48 minutes (red curve) and after 150 minutes (blue curve) of contact with the flue gas. Transition spectra (light grey curves) were acquired every 10 minutes. Blue stars label the main spectral features appearing as a consequence of the long contact with CO_2. Section (c): CO_2 breakthrough curve collected monitoring the gas phase during the whole experiment. The first dashed line (t=0 min) marks the beginning of the synthetic flue gas bubbling inside the DMSO/IL solution and refers to the black spectrum in section (a). The second dashed line (t=48 min) corresponds to the transition from section (a) to section (b).

Figure 3a reports the spectrum of the DMSO-[Cho][Gly] solution (black curve) before contact with CO_2. The spectral features of [Cho][Gly] are all recognizable, as described in detail in Figure 2a and in Table 1. Beside the bands of the bare IL, the signals of the solvent are easily distinguishable (see for comparison the black dotted spectrum of pure DMSO reported in Figure 3a).

After the baseline acquisition by means of the dedicated bypass line, as described in the experimental section, the gas flow was bubbled through the IL solution inside the mixing chamber at t = 0 min. Exactly at that time, as shown in Figure 3c, the breakthrough curve suddenly drops to zero, testifying that the [Cho][Gly]-DMSO solution is sequestrating CO_2 from the gas stream. The black spectrum of Figure 3a remains obviously unchanged, until the flue gas is directed through the IL solution at t = 0 min. From that moment, indeed, the spectrum of the [Cho][Gly]-DMSO solution undergoes evident modifications, with the appearance of new spectral features that, after a starting induction period (probably essential for the diffusion of the gas into the bulk liquid phase), rapidly increase in intensity. After 48 minutes of contact with the flue gas, these new bands (identified by the red stars in Figure 3a) become well evident in the spectrum. In particular, the band located at around 1600 cm^{-1} in the spectrum of the bare IL becomes broader and more intense due to the appearance of two new signals at around 1625 and 1525 cm^{-1} related to the formation of NH_3^+ species. In parallel, the new bands at 1380 cm^{-1} and 1312 cm^{-1} points out the generation of the carbamate moiety (-NHCOO). [49] The amino groups of two adjacent glycinate anions react with the CO_2 through a cooperative 2:1 mechanism,[52] as reported in Scheme 3, process (i) to (ii). In particular, the first amine reacts with CO_2 generating a carbamate species, while a proton moves to the second amine forming the ammonium counterion. It is worth noticing that one of the two glycines, that extracts a proton from a neighboring amine to favor the insertion of the CO_2 molecule, giving rise to an NH_3^+ moiety, transforms into a z-glycine. It is also important to highlight that a consistent fraction of CO_2 is absorbed by the IL in the first 50 minutes of reaction and that, exactly when the carbamate species stop forming, the breakthrough curve changes concavity (see Figure 3c). From this point, the CO_2 concentration in the gas stream slowly increases again, tending to an almost constant value after 2 hours of reaction.

In Figure 3b the ATR-IR spectra collected between 48 and 150 minutes of reaction are reported. Immediately after 48 minutes of contact with the synthetic flue gas, the spectral features of the just formed carbamate species start to decrease. After 150 minutes, simultaneously to the almost total disappearance of the bands ascribable to the carbamate moieties, new signals arise in the spectrum at 1698 cm^{-1}, 1520 and 1380 cm^{-1} (see blue spectrum in Figure 3b and bands labeled with blue stars). These spectral modifications can be unequivocally ascribed to the formation of carbamic acid. [53–56]

Considering that the carbamate signals decrease when the carbamic acid features appear, it is possible to assume a conversion of the ammonium carbamate species into carbamic acid through a proton transfer as depicted in Scheme 3, process (ii) to (iii). In principle, carbamic acid can be formed also through an intramolecular path, where a proton is transferred from the amine directly to the carbamate (*i.e.* with a 1:1 mechanism in one step, process (i) to (iii), grey arrow in Scheme 3). This mechanism does not require the

presence of adjacent glycine anions to preliminary form the NH_3^+ moiety, thus if the formation of carbamic acid preferentially occurs through this reaction way the formation of NH_3^+ should be limited. Since the intensity of the vibrational features of NH_3^+ increase along the first 48 min of reaction and then decreases upon the formation of carbamic acid, the intramolecular mechanism seems to be not favored for [Cho][Gly] under these reaction conditions.
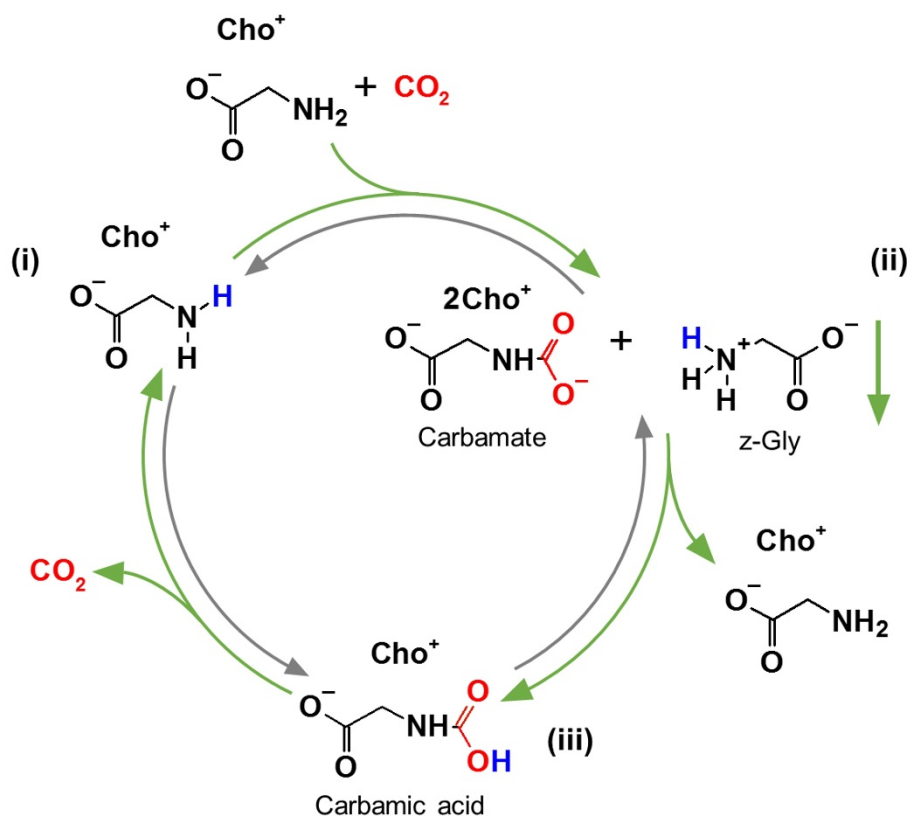
Scheme 3 Reaction paths between [Cho][Gly] and CO_2. Observed reactions are indicated by green arrows. Possible reactions without experimental evidences are labeled with the grey arrows.

Table 3 Assignments of the main FT-IR bands formed upon CO_2 absorption in [Cho][Gly]-DMSO solution (see Figures 3a and 3b).

Wavenumber[a]	Assignment	Ref.
1698 [b]	C=O stretching of carbamic acid	[53,55–57]
1625-1525 [c]	Asymmetric and symmetric NH_3^+ bending	[50,58]
1584-1380 [c]	Asymmetric and symmetric carbamate COO^- stretching	[55,56]
1520 [b]	CN stretching and NH bending of carbamic acid	[53,56,59,60]
1380 [b]	OH bending of carbamic acid	[56,59]
1312 [c]	$NCOO^-$ skeletal vibration	[56]

[a] wavenumber (in cm^{-1}) from this work.
[b] signal present in the blue spectrum of Figure 3b.
[c] signal present in the red spectrum of Figure 3a and Figure 3b.

For the sake of simplicity, the main FT-IR bands, deriving from the species that form during the reaction of the [Cho][Gly]-DMSO solution with CO_2, are listed in Table 3.

As proved by the breakthrough curve (Figure 3c), after 150 minutes of reaction, the CO_2 concentration in the gas stream reaches an almost constant value, testifying that the IL saturation occurs.

At that time, the gas stream was directed into the bypass line and the gas composition was changed into pure N_2. A new baseline was collected, then the gas was bubbled again inside the mixing chamber, to favor the release of CO_2 from the bulk liquid phase. Figure 4a reports the ATR-IR spectra evolution, in the 1800-1100 cm^{-1} range, during the desorption run. The corresponding CO_2 concentration trend is displayed in Figure 4b. As soon as the release process begins, the CO_2 concentration immediately raises, to then decrease reaching a value close to zero after 200 minutes. However, by comparing the CO_2 breakthrough curve during the absorption run (Figure 3c) with the CO_2 concentration trend during the desorption one (Figure 4b), it is clear that only a fraction of the molecule is released by the liquid. The partial desorption is confirmed by the ATR-IR spectra collected on the [Cho][Gly]-DMSO solution during the N_2 bubbling, as reported in Figure 4a. Indeed, throughout the CO_2 release, the carbamic acid fingerprints at 1698 cm^{-1}, 1520 and 1380 cm^{-1} gradually disappear. After 550 minutes of desorption (see dark cyan spectrum in Figure 4a), the signals of carbamic acid are virtually absent, whereas some residual spectral features of ammonium carbamate species return to be visible, as labeled by the red and cyan stars in Figure 4a. However, the intensity of these species is definitely lower if compared withthe spectra collected during the first stages of the CO_2 uptake (compare the dark cyan spectrum in Figure 4a with the red spectrum in Figure 3a). Moreover, the spectra collected during desorption shows as a direct conversion of carbamic acid into carbamate species (process (iii) to (ii) in Scheme 3) does not occur preferentially, despite the disappearance of the carbamic acid signals during the desorption process. This latter species is, in fact, not sufficiently stable to survive without a CO_2 excess. In order to explain the absence of the carbamic acid bands in the spectrum collected at the end of the desorption run and the partial release of CO_2 observable in the breakthrough curve of Figure 4b, the conversion mechanism reported in Scheme 3, process (iii) to (i), could be proposed. Considering this pathway, the carbamic acid converts in the starting IL by simply releasing CO_2. The signals of the restored IL are not visible in the spectra collected at the end of the desorption run due to the overlapping of the bands generated by the residual fraction of ammonium carbamate.

Nevertheless, beside this partial reversible behavior, unfortunately [Cho][Gly] undergoes an irreversible transformation during the CO_2 absorption. Indeed, already in the early stages of the experiment, the [Cho][Gly]-DMSO solution loses its clearness due to the formation of a white precipitate. The precipitate revealed to be solid glycine. In fact, considering the results obtained in another experiment (performed with a more concentrated [Cho][Gly]-DMSO 1:2 volume ratio solution) the ATR-IR spectra, collected during the CO_2 absorption/desorption runs, exhibit the typical spectral features of solid glycine in both neutral and zwitterionic form [50], as displayed in Figure S3 of the Supplementary Material. The precipitation of solid glycine probably occurs in the first step of the absorption, during the formation of the carbamate species (see (ii) in Scheme 3),

when one of the two glycinate anions involved in the process, extracting a proton from a neighboring amine to favor the insertion of the CO_2 molecule, transforms into z-glycine. The low solubility of the z-glycine in DMSO is probably responsible for the precipitation of the solid. This irreversible chemical modification of the IL does not allow the same [Cho][Gly]-DMSO solution to be employed in a second absorption/desorption cycle.
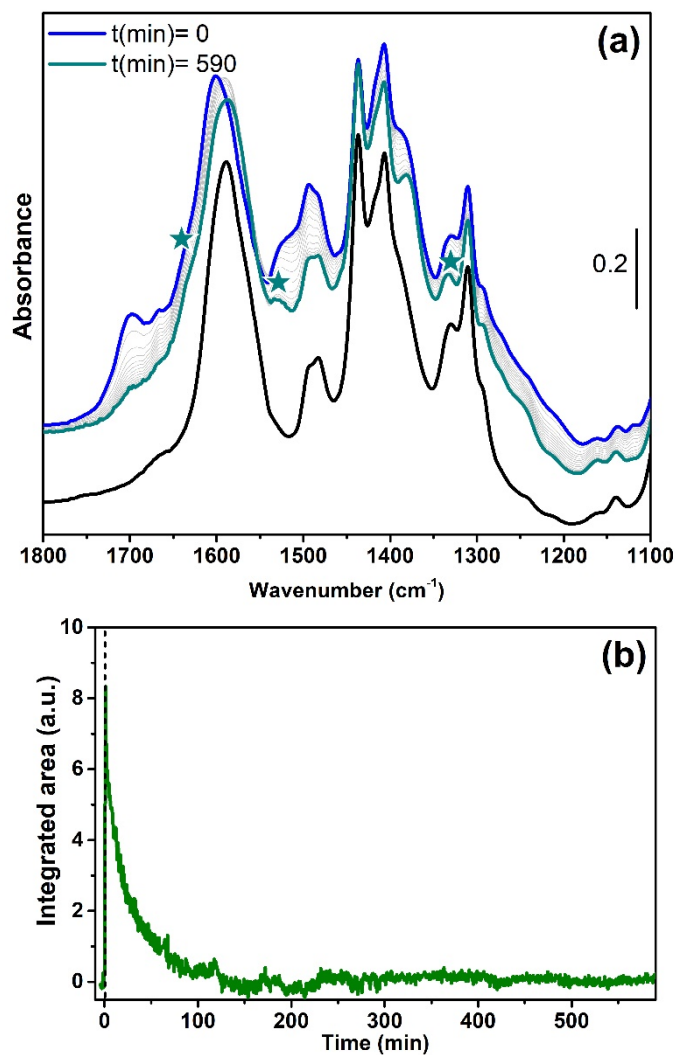
Figure 4 Section (a): time evolution of the ATR-IR spectra, in the 1800-1100 cm^{-1} spectral region, of the [Cho][Gly]-DMSO solution during the desorption run, *i.e.* bubbling a N_2 stream inside the mixing chamber. ATR-IR spectra of [Cho][Gly]-DMSO solution before CO_2 absorption (black curve), of the [Cho][Gly]-DMSO solution after 150 minutes (blue curve) of contact with the flue gas and after 590 minutes of contact with a N_2 stream (dark cyan line). Transition spectra (light grey curves) were acquired every 30 minutes. Dark cyan and red stars label the main spectral features of the ammonium carbamate species present in the dark cyan spectrum. Section (b): CO_2 concentration curve collected monitoring the gas phase during the N_2 bubbling inside the [Cho][Gly]-DMSO solution. The dashed line (t=0 min) marks the beginning of the N_2 bubbling and corresponds to the blue spectrum in section (a).

### 3.3.2 CO$_2$ absorption in [Cho][Pro]-DMSO solution.

In the second experiment, the CO$_2$ absorption in the [Cho][Pro]-DMSO solution (16%wt/wt) has been studied. Figure 5a reports the ATR-IR spectra of the [Cho][Pro]-DMSO solution in the different stages of the CO$_2$ absorption process, in the 1800-1100 cm^{-1} spectral range. The corresponding breakthrough curve are shown in Figure 5b. The synthetic flue gas was directed inside the mixing chamber, after the usual baseline acquisition. Similarly to the first experiment, the CO$_2$ concentration rapidly drops to zero in the early stages of the experiment (see Figure 5b), testifying the CO$_2$ sequestration ability of the [Cho][Pro]-DMSO solution. At the same time, the ATR-IR spectrum of the [Cho][Pro]-DMSO solution starts changing, as reported in Figure 5a.
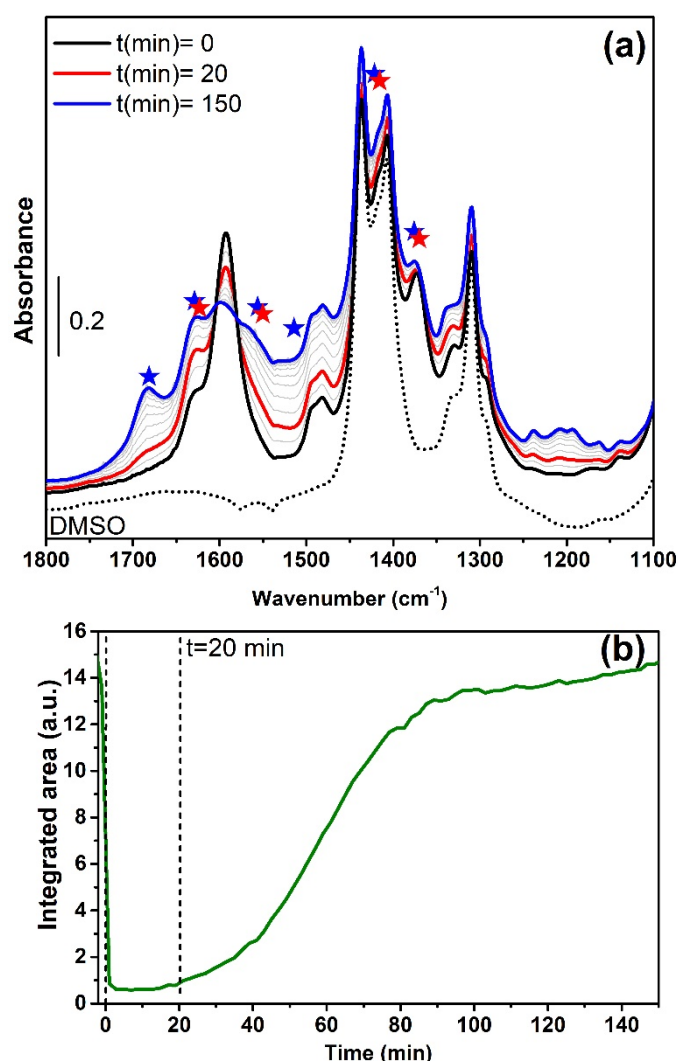
Figure 5 Section (a): time evolution of the ATR-IR spectra, in the 1800-1100 cm^{-1} spectral region, of [Cho][Pro]-DMSO 16%wt/wt solution in contact with the synthetic flue gas (composition: 20 vol% CO$_2$ in N$_2$). ATR-IR spectra of pure DMSO (black dotted curve), [Cho][Pro]-DMSO solution (black curve), [Cho][Pro]-DMSO solution after 20 (red curve) and 150 minutes (blue curve) of contact with the flue gas. Transition spectra (light grey curves) were acquired every 10 minutes. Red and blue stars label the main spectral features appearing consequently to the CO$_2$ interaction. Section (b): CO$_2$ breakthrough

curve collected monitoring the gas phase during the CO_2/N_2 mixture bubbling. The first dashed line (t=0 min) marks the beginning of the synthetic flue gas bubbling inside the DMSO/IL solution and corresponds to the black spectrum in section (a). The second dashed line (t=20 min) refers to the red spectrum in section (a).

In fact, as soon as the CO_2 is bubbled in the IL solution, the band related to the [Cho][Pro] carboxylate group asymmetric stretching vibration at 1590 cm^{-1} decreases in intensity and, in parallel, new spectral features appear at 1554-1381 cm^{-1} and at 1628-1407 cm^{-1} generated by the NH_2^+ and the OCO^- moieties of carbamate species respectively. [51,60] As already observed for [Cho][Gly], the amino groups of two adjacent prolines react with the CO_2 through a cooperative 2:1 mechanism (see Scheme 4, process (i) to (ii)).
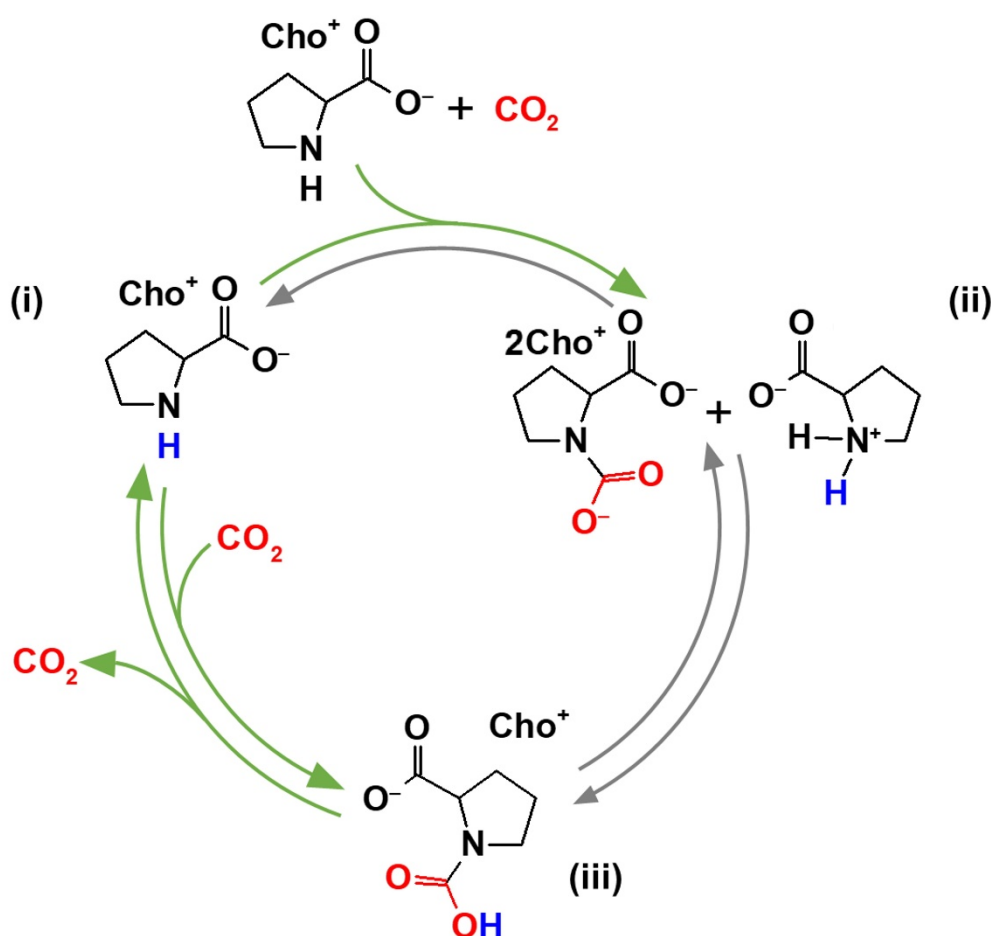
Scheme 4 Reaction paths between [Cho][Pro] and CO_2. Observed reactions are indicated by green arrows. Possible reactions without experimental evidences are labeled with the grey arrows.

After a brief starting period (within the first 20 minutes of reaction), other signals rapidly increase simultaneously to the fingerprints of the carbamate species. These bands can be ascribed to the C=O stretching mode (signal at 1683 cm^{-1}) and to the CN stretching vibration (band at 1520 cm^{-1}) of carbamic acid.

It is worth noting that, in contrast to what observed in the presence of the [Cho][Gly]-DMSO solution, the formation of the carbamic acid begins earlier, when the CO_2 is still closely fully absorbed by the IL, as proved by the breakthrough curves (see the dashed line at t = 20 min in Figure 5b).

The infrared data clearly prove that, in the presence of [Cho][Pro], the CO_2 absorption occurs through two different mechanisms that take place simultaneously without any interconversion between the ammonium carbamate species and the carbamic acid (Scheme 4, processes (i) to (ii) and (i) to (iii)). Indeed, differently from [Cho][Gly] (in which the ammonium carbamate, formed in the early stages of the absorption, convert into carbamic acid following the mechanism reported in Scheme 3, process (ii) to (iii)), in the presence of [Cho][Pro], the carbamic acid and ammonium-carbamate species seem to evolve independently. Therefore, it is possible to assume 1:1 mechanism in one step for the carbamic acid formation, *i.e.* through the direct reaction of just one proline with a CO_2 molecule (path (i) to (iii) in Scheme 4).

The main FT-IR bands of the different species that appear consequently to the chemical reactivity between the [Cho][Pro]-DMSO solution and CO_2 are listed in Table 4.

Table 4 Assignments of the main FT-IR bands formed upon CO_2 absorption in [Cho][Pro]-DMSO solution (see Figure 5a).

Wavenumber[a]	Assignment	Ref.
1683[b]	C=O stretching of carbamic acid	[39,53,56,57,60]
1628-1407 [b]	Asymmetric and symmetric carbamate COO^- stretching	[55,56]
1554-1381 [b]	Asymmetric and symmetric NH_2^+ bending	[51]
1520 [b]	CN stretching of carbamic acid	[53,56,59,60]
1380 [b]	OH bending of carbamic acid	[56,59,61]
1312 [b]	$NCOO^-$ skeletal vibration	[56,62]

[a] wavenumber (in cm^{-1}) from this work
[b] signals present in both red and blue spectra of Figure 5a.

As proved by the breakthrough curve (Figure 5b), after 150 minutes of reaction, the CO_2 concentration in the gas stream reaches an almost constant value, due to the saturation of the IL. At that time, the gas stream was directed into the bypass line and the gas composition was changed into pure N_2. A new baseline was collected and the gas was bubbled again inside the mixing chamber, to favor the release of CO_2 from the bulk liquid phase. Figure 6a reports the ATR-IR spectra of the [Cho][Pro]-DMSO solution during the desorption run, in the 1800-1100 cm^{-1} spectral range. Figure 6b shows the corresponding CO_2 concentration curve.

When pure N_2 is bubbled inside the IL solution, a fraction of CO_2 is released by the bulk liquid. The CO_2 concentration trend reported in Figure 6b, shows a faster release in the first 40 minutes, followed by a slower decrease of the CO_2 concentration to reach a value close to zero after 500 minutes.

As for [Cho][Gly], only a fraction of CO_2 is actually released by [Cho][Pro]. The partial desorption is confirmed by the ATR-IR spectra evolution collected on the [Cho][Pro]-

DMSO solution during the N_2 bubbling, as reported in Figure 6a. The carbamic acid spectral features gradually disappear during the desorption run, whereas the bands of the original IL (see for example the signal at 1590 cm^{-1} due to the asymmetric OCO$^-$ stretching vibration of [Cho][Pro]) increase again in intensity. These spectral modifications confirm that prolinate anions of the IL are partially restored. On the other hand, the spectral features related to the ammonium-carbamate species just slightly decrease during the desorption run. This spectral behavior again suggest CO_2 is easily released from carbamic acid through the direct restoring of the IL (path (iii) to (i) in Scheme 4). In contrast to the IL containing glycine, when the proline moiety is present, the reaction of CO_2 with the IL to give carbamic acid (as well as the reverse process) does not occur *via* an ammonium-to-carbamate proton transfer. The heterocyclic ring of proline could be responsible for this different behavior, contributing to partially segregate the amine moieties, so favoring the direct reaction of CO_2 with only one amine and generating carbamic acid through a 1:1 mechanism in one step. In future works, insights from molecular modeling will represent a valuable tool to fully confirm this peculiar mechanism.

Summarizing, in the case of [Cho][Pro] two different reaction mechanisms can be supposed, as reported in Scheme 4: a faster and irreversible formation of ammonium-carbamate couples ((i) to (ii) path) and a slower and reversible formation of carbamic acid ((i) to (iii) route and vice versa).

It is worth noting that, during the whole CO_2 absorption/desorption experiment with [Cho][Pro], the solution remains clear and no precipitate is observed due probably to the higher solubility in DMSO of the z-proline formed during the reaction ((ii) in Scheme 4).
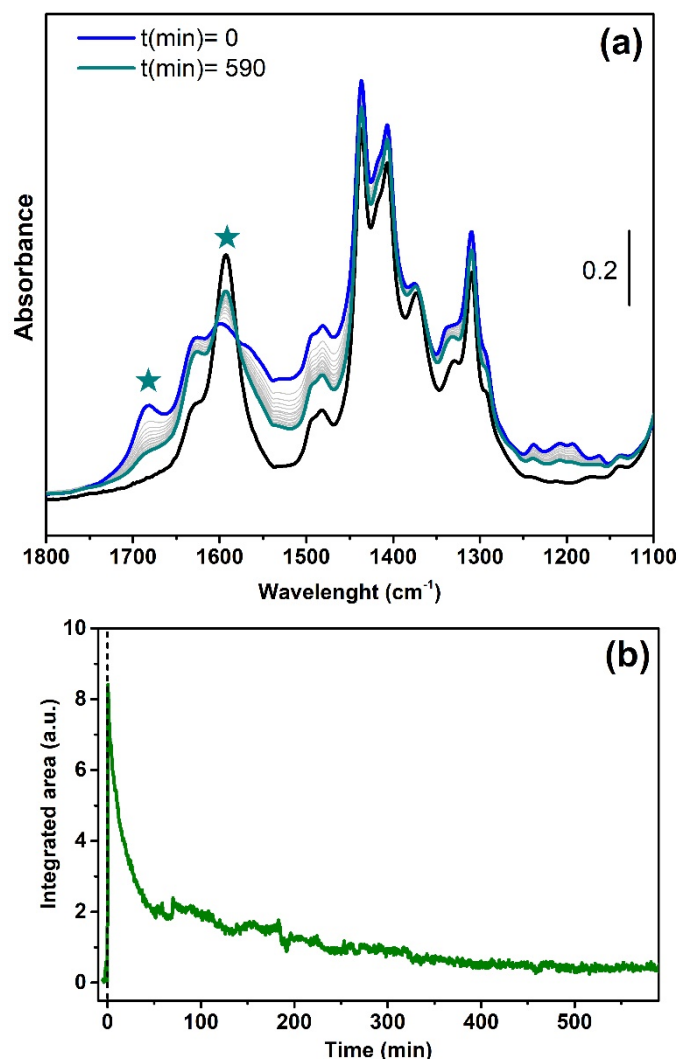
Figure 6 Section (a): time evolution of the ATR-IR spectra, in the 1800-1100 cm^{-1} spectral region, of [Cho][Pro]-DMSO solution during the desorption run, *i.e.* bubbling N$_2$ inside the mixing chamber. ATR-IR spectra of the [Cho][Pro]-DMSO solution before CO$_2$ absorption (black curve), of the [Cho][Pro]-DMSO solution after 150 minutes (blue curve) of contact with the flue gas and after 550 minutes of contact with a N$_2$ stream (dark cyan line). Transition spectra (light grey curves) were acquired every 30 minutes. Dark cyan stars label the relevant spectral features changes in the spectrum collected at the end of the desorption process. Section (b): CO$_2$ concentration curve collected monitoring the gas phase during the N$_2$ bubbling in the [Cho][Pro]-DMSO solution. The dashed line (t=0 min) marks the beginning of the N$_2$ bubbling and and corresponds to the blue spectrum in section (a).

The excellent stability of [Cho][Pro] has been exploited to perform an additional absorption run in order to confirm the actual reversibility of the carbamic acid formation *via* 1:1 mechanism in one step ((i) to (iii) process in Scheme 4). To this purpose, the synthetic flue gas was fluxed again in the mixing chamber for a shorter time (~60 minutes).

Figure 7 reports the ATR-IR spectra collected on the [Cho][Pro]-DMSO solution during the secondary absorption run: dark cyan and blue spectra have been collected at t = 0 min and at t = 60 min respectively. The inset reports the corresponding CO_2 breakthrough curve. The carbamic acid formation can be explicitly observed after 60 minutes (see bands at 1683, 1520 and 1380 cm^{-1}). In parallel to the formation of the carbamic acid, the main signal of the bare IL at 1590 cm^{-1} decreases in intensity. In addition, there is no evidence of further formation of ammonium-carbamate couples. The CO_2 breakthrough curve is instead very different from the primary absorption run: the CO_2 concentration does not drop to zero, testifying a reduced absorption capacity of the solution. Moreover, the CO_2 concentration level comes back to the initial value in less time with respect to the first run (~40 minutes instead of ~100 minutes).

It is evident that, at the end of the first cycle, the [Cho][Pro] solution does not fully recover its starting absorption performances and only the reversible formation of carbamic acid is responsible for the residual absorption capacity of this IL.
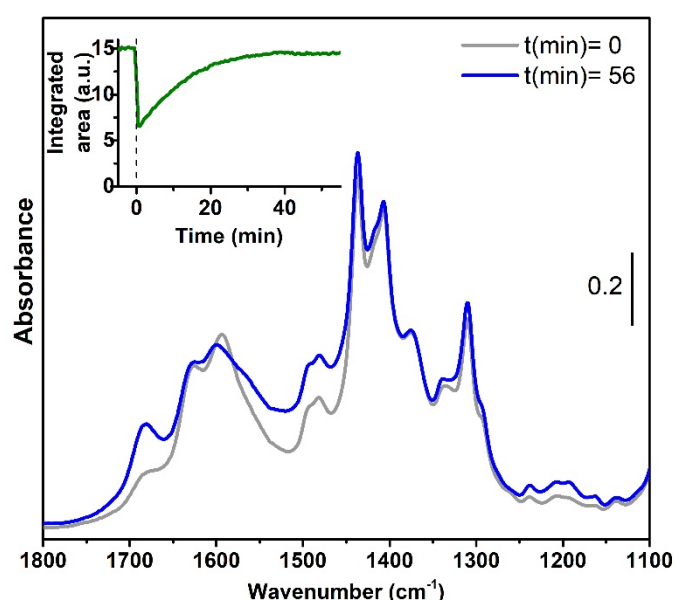
Figure 7 ATR-IR spectra, in the 1800-1100 cm^{-1} spectral region, of the [Cho][Pro]-DMSO solution during the second absorption run. ATR-IR spectra of the [Cho][Pro]-DMSO solution at the end of the first cycle (grey curve) and of the [Cho][Pro]-DMSO solution after 60 minutes (blue curve) of contact with the flue gas.

3.4 Study of temperature effects on the CO_2 absorption/desorption processes

The operando FT-IR study has been integrated, as requested by one of the reviewers, with some additional quantitative measurements. These supplementary analyses have been performed through a dedicated apparatus, allowing the investigation of the temperature effects on CO_2 absorption/desorption processes. In particular, we focused on a [Cho][Pro]-DMSO 16%wt/wt solution. [Cho][Pro] was selected to perform these experiments because it does not irreversibly alter during the CO_2 absorption process.

At first, the AC and ME of the [Cho][Pro]-DMSO solution were evaluated at different temperature: 25°C, 30°C and 40°C. It is worth noting that the results displayed in Table 5 are consistent with the quantification reported in Section 3.2. Both the AC and the ME decreases as temperature increases. This behavior is in agreement with the information obtained from the *operando* spectroscopy experiment. Indeed, the formation of carbamic acid, which revealed to be labile and reversible, could be partially inhibited at higher temperature, thus leading to the decrease of the AC and ME values.

Table 5 CO_2 absorption performance of [Cho][Pro]-DMSO solution 16%wt/wt at different temperatures.

Absorption temperature (°C)	AC[a]	ME[b]
25	2.39 ± 0.24	0.74 ± 0.07
30	2.27 ± 0.22	0.71 ± 0.07
40	2.14 ± 0.21	0.66 ± 0.07

[a] Absorption capacity, expressed as %wt(CO_2)/wt(solution)
[b] Molar efficiency, expressed as mol(CO_2)/mol(IL)

Beside adsorption, the CO_2 desorption at temperature higher than RT was investigated too. A CO_2 capture-release experiment was carried out on the 16%wt/wt solution of [Cho][Pro] in DMSO: the overall evolution of the experiment is depicted in Figure 8, where the variations of temperature (red curve), CO_2 concentration (green curve) and adsorbed CO_2 (black curve) are reported. After an initial purging with N_2 (40 ml/min) during a pre-heating stage up to the desired absorption temperature (30 °C, see Fig. 8(i)), the CO_2 absorption step was performed (see Fig. 8 section (ii), gas flow 40ml/min, 20%v/v of CO_2 in N_2), maintaining the sample exposed to the flue gas until saturation occurred. The desorption process, entirely carried under 40 ml/min of N_2, was instead divided into two steps: in the first 10 min the sample was maintained at 30°C (see Fig.8 section (iii)) to evaluate the extent of desorption in this condition, then the temperature was risen up to 80°C with a ramp of 5°C/min (see Fig.8 section (iv)) to study the desorption capacity of the system at increased temperatures.

Concerning the desorption step, similarly to the case of FT-IR *operando* experiments, the CO_2 concentration (green curve in Fig.8) suddenly drops towards zero, but not all the CO_2 absorbed is released (black curve in Fig.8). Conversely, the CO_2 is fully released upon heating. Although the maximum in the CO_2 concentration profile is observed at ~65-70°C, the CO_2 releasing process begins at an even lower temperature (~50°C). This experiment clearly demonstrates that the total release of the captured CO_2 is achievable at mild temperatures and that the ammonium-carbamate species (not reversible at RT, as proved by the *operando* IR experiments) become significantly unstable at ~70°C. It is worth noting that, with respect to the classical aqueous amine solutions (requiring temperatures higher than 100°C to achieve a complete CO_2 release), these bio-inspired ILs are able to totally desorb CO_2 at definitely lower temperatures.
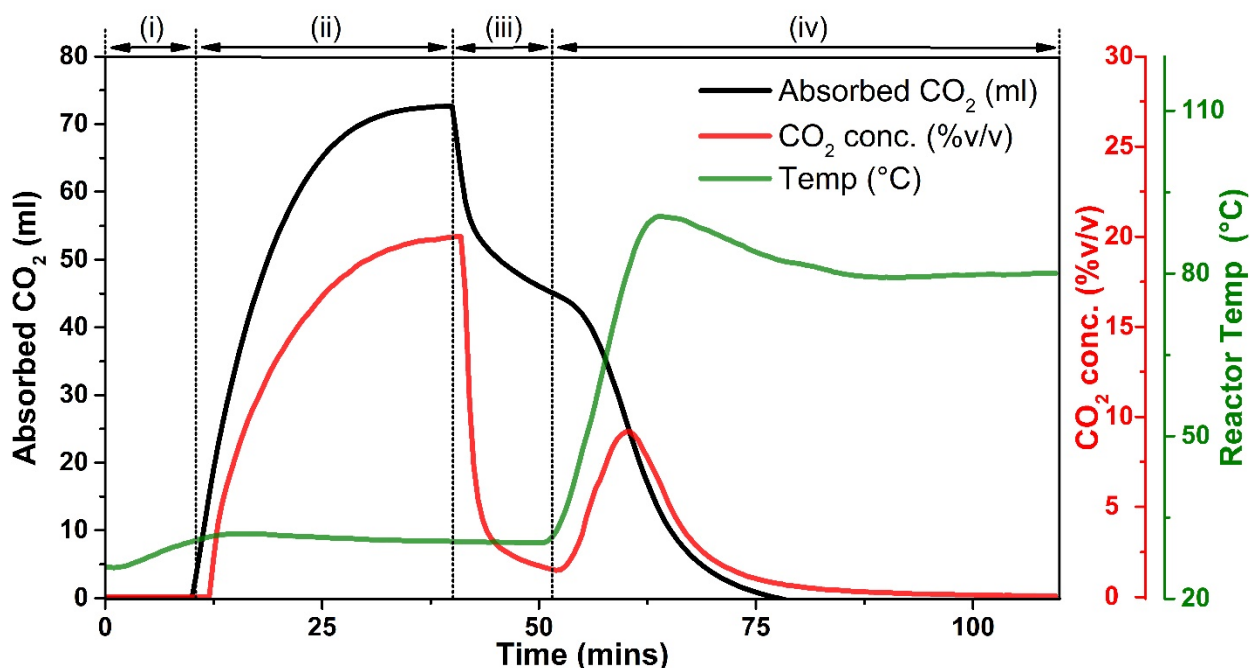
Figure 8 Evolution of the CO_2 capture-release experiment in the presence of a [Cho][Pro]-DMSO (16%wt/wt) solution: the the variations of temperature (red curve), CO_2 concentration (green curve) and adsorbed CO_2 (black curve) are reported. The experiment is divided into four steps: pre-heating to 30°C (section (i), gas flow 40ml/min N_2), absorption at 30°C (section (ii), gas flow 40ml/min, 20%v/v CO_2 in N_2), desorption at 30°C (section (iii), gas flow 40ml/min N_2) and desorption upon heating at 80°C (section (iv), gas flow 40ml/min N_2).

4. Conclusions

This work presented an innovative synthetic method for preparing choline-AAILs and their advanced study during the CO_2 absorption through operando IR spectroscopy. In detail, we proposed a synthetic procedure exploiting a choline salt (namely choline chloride) rather than the conventional hydroxide precursor, thus limiting the drawback related to handling the highly basic and reactive choline hydroxide. Two different choline-AAILs, based on glycine and proline amino acids, were synthesized: [Cho][Gly] and [Cho][Pro] respectively. Both ILs were spectroscopically investigated by means of ATR-IR spectroscopy, also during the contact with a synthetic flue gas (20 %v/v of CO_2 in N_2). Even though elementary reactions are the same for all the investigated systems, different overall absorption pathways were recognized depending on the amino acid based anion. The fresh [Cho][Gly]-DMSO solution effectively absorbs CO_2 through the formation of ammonium carbamate species, *i.e.* with a 2:1 mechanism. Only at long contact time, ammonium carbamate is partially converted into carbamic acid through a proton transfer from the ammonium to the carbamate. During the desorption stage, only a fraction of the absorbed CO_2 is released as corroborated by the collected breakthrough curves. The ATR-IR analysis of the [Cho][Gly]-DMSO solution during this stage further showed as the released CO_2 mostly originates form the direct decomposition of the carbamic acid to give the bare IL, *i.e.* without implying an

intermediate formation of ammonium carbamate species. Noteworthy, from the early stages of the absorption process, a white precipitate (recognized as solid glycine) forms within the solution. Such behavior, irreversibly altering the IL, can be ascribed to the formation of z-glycine as the ammonium counterion of the carbamate species that, due to its low solubility in DMSO, precipitates. [Cho][Pro] exhibits a partly different absorption behavior: the formation of carbamic acid does not takes place from a proton transfer from ammonium to carbamate species (which are however experimentally observed in the solution) species as in [Cho][Gly], instead it forms from the direct reaction of CO_2 with a single prolinate anions with a 1:1 mechanism in one step. Another relevant difference in the absorption step is the absence of precipitate phases, probably ascribed to the higher solubility of z-proline in DMSO compared to z-glycine. Concerning the desorption stage, [Cho][Pro] follows the same mechanism proposed for [Cho][Gly], with the direct decomposition of carbamic acid to CO_2 and bare IL. The ammonium carbamate species again exhibit high stability and are only partially degraded in absence of CO_2 in the gaseous stream. Since the absorption/desorption cycle did not irreversibly alter the IL, a secondary absorption run has been performed on [Cho][Pro]. Compared to the primary one, the secondary absorption showed a significantly reduced absorption capacity of the IL/DMSO system. Indeed, in the secondary absorption cycle the CO_2 absorption process occurs only thanks to the direct formation of carbamic acid through a 1:1 mechanism in one step.

The insights obtained from the operando ATR-IR approach presented in this work demonstrates the importance of this type of investigation in the understanding of reactivity under realistic working conditions. Even though both ILs showed similar absorption capabilities, the elementary reactions driving the process differ between them. Thus, the selection of different AA based anions significantly affects the performances of the resulting IL. Future work will focus on the screening of selected AAs, in order to clearly define structure-properties relationship useful to the rational design of improved choline-AAILs for CO_2 capture. Moreover, the preliminary results obtained by the absorption/desorption quantitative evaluation proved how these bio-inspired ILs are very promising alternatives to the classical aqueous amine technology, mainly thanks to their significantly lower CO_2 release temperature.

Acknowledgements

References

[1]   F.B. France, U. Cubasch, P.F. Uk, P. Friedlingstein, P.C. France, M.C. Uk, C. Josefino, IPCC, Climate Change 2013: The Physical Science Basis - Summary for Policymakers, Observed Changes in the Climate System, IPCC. (2013) 15. http://www.climatechange2013.org/images/report/WG1AR5_SPM_FINAL.pdf.

[2]   G.A. Schmidt, R.A. Ruedy, R.L. Miller, A.A. Lacis, Attribution of the present-day total greenhouse effect, J. Geophys. Res. Atmos. 115 (2010) D20106.

doi:10.1029/2010JD014287.

[3]   A.H.F. Li, Hopes of limiting global warming?: China and the Paris agreement on climate change, China Perspect. 1 (2016) 49–54. http://www.cefc.com.hk/article/hopes-of-limiting-global-warming-china-and-the-paris-agreement-on-climate-change/.

[4]   Record annual increase of carbon dioxide observed at Mauna Loa for 2015, (n.d.). www.noaa.gov/record-annual-increase-carbon-dioxide-observed-mauna-loa-2015 (accessed June 21, 2017).

[5]   S. Bocchini, C. Castro, M. Cocuzza, S. Ferrero, G. Latini, A. Martis, F. Pirri, L. Scaltrito, V. Rocca, F. Verga, D. Viberti, The Virtuous CO 2 Circle or the Three Cs: Capture, Cache, and Convert, J. Nanomater. 2017 (2017) 1–14. doi:10.1155/2017/6594151.

[6]   G.T. Rochelle, Amine Scrubbing for CO2 Capture, Science (80-.). 325 (2009) 1652–1654. doi:10.1126/science.1176731.

[7]   C.W. Jones, CO2 Capture from Dilute Gases as a Component of Modern Global Carbon Management, Annu. Rev. Chem. Biomol. Eng. 2 (2011) 31–52. doi:10.1146/annurev-chembioeng-061010-114252.

[8]   P.M.M. Blauwhoff, G.F. Versteeg, W.P.M. Van Swaaij, A study on the reaction between CO2 and alkanolamines in aqueous solutions, Chem. Eng. Sci. 39 (1984) 207–225. doi:http://dx.doi.org/10.1016/0009-2509(84)80021-4.

[9]   B. Arstad, R. Blom, O. Swang, CO2 Absorption in Aqueous Solutions of Alkanolamines: Mechanistic Insight from Quantum Chemical Calculations, J. Phys. Chem. A. 111 (2007) 1222–1228. doi:10.1021/jp065301v.

[10]   D. Barth, C. Tondre, G. Lappai, J.J. Delpuech, Kinetic study of carbon dioxide reaction with tertiary amines in aqueous solutions, J. Phys. Chem. 85 (1981) 3660–3667. doi:10.1021/j150624a027.

[11]   C. Song, Global challenges and strategies for control, conversion and utilization of CO2 for sustainable development involving energy, catalysis, adsorption and chemical processing, Catal. Today. 115 (2006) 2–32. doi:https://doi.org/10.1016/j.cattod.2006.02.029.

[12]   T. Sakakura, J.-C. Choi, H. Yasuda, Transformation of Carbon Dioxide, Chem. Rev. 107 (2007) 2365–2387. doi:10.1021/cr068357u.

[13]   E.A. Quadrelli, G. Centi, J.L. Duplan, S. Perathoner, Carbon dioxide recycling: Emerging large-scale technologies with industrial potential, ChemSusChem. 4 (2011) 1194–1215. doi:10.1002/cssc.201100473.

[14]   D.A. Palmer, R. Van Eldik, The chemistry of metal carbonato and carbon dioxide complexes, Chem. Rev. 83 (1983) 651–731. doi:10.1021/cr00058a004.

[15]   G. Centi, E.A. Quadrelli, S. Perathoner, Catalysis for CO2 conversion: a key technology for rapid introduction of renewable energy in the value chain of chemical industries, Energy Environ. Sci. 6 (2013) 1711–1731. doi:10.1039/C3EE00056G.

[16]   M. Aresta, A. Dibenedetto, A. Angelini, Catalysis for the valorization of exhaust carbon: From CO2to chemicals, materials, and fuels. technological use of CO2, Chem. Rev. 114 (2014) 1709–1742. doi:10.1021/cr4002758.

[17]   P. Walden, Ueber die Molekulargrösse und elektrische Leitfähigkeit einiger geschmolzenen Salze, Bull. l'Académie Impériale Des Sci. St.-Pétersbourg. VI Série. 8 (1914) 405–422.

[18]   N. V. Plechkova, K.R. Seddon, Applications of ionic liquids in the chemical industry, Chem. Soc. Rev. 37 (2008) 123–150. doi:10.1039/b006677j.

[19]   Z.-Z. Yang, Y.-N. Zhao, L.-N. He, CO2 chemistry: task-specific ionic liquids for CO2

capture/activation and subsequent conversion, RSC Adv. 1 (2011) 545. doi:10.1039/c1ra00307k.

[20]   S. Sarmad, J.-P. Mikkola, X. Ji, Carbon Dioxide Capture with Ionic Liquids and Deep Eutectic Solvents: A New Generation of Sorbents, ChemSusChem. 10 (2017) 324–352. doi:10.1002/cssc.201600987.

[21]   S. Zeng, X. Zhang, L. Bai, X. Zhang, H. Wang, J. Wang, D. Bao, M. Li, X. Liu, S. Zhang, Ionic-Liquid-Based CO_2 Capture Systems: Structure, Interaction and Process, Chem. Rev. 117 (2017) 9625–9673. doi:10.1021/acs.chemrev.7b00072.

[22]   G. Cui, J. Wang, S. Zhang, Active chemisorption sites in functionalized ionic liquids for carbon capture, Chem. Soc. Rev. 45 (2016) 4307–4339. doi:10.1039/C5CS00462D.

[23]   J.P. Hallett, T. Welton, Room-Temperature Ionic Liquids: Solvents for Synthesis and Catalysis. 2, Chem. Rev. 111 (2011) 3508–3576. doi:10.1021/cr1003248.

[24]   R.D. Rogers, CHEMISTRY: Ionic Liquids--Solvents of the Future?, Science (80-.). 302 (2003) 792–793. doi:10.1126/science.1090313.

[25]   H. Olivier-Bourbigou, L. Magna, D. Morvan, Ionic liquids and catalysis: Recent progress from knowledge to applications, Appl. Catal. A Gen. 373 (2010) 1–56. doi:http://dx.doi.org/10.1016/j.apcata.2009.10.008.

[26]   C. Verma, I.B. Obot, I. Bahadur, E.-S.M. Sherif, E.E. Ebenso, Choline based ionic liquids as sustainable corrosion inhibitors on mild steel surface in acidic medium: Gravimetric, electrochemical, surface morphology, DFT and Monte Carlo simulation studies, Appl. Surf. Sci. 457 (2018) 134–149. doi:https://doi.org/10.1016/j.apsusc.2018.06.035.

[27]   C. Verma, E.E. Ebenso, M.A. Quraishi, Corrosion inhibitors for ferrous and non-ferrous metals and alloys in ionic sodium chloride solutions: A review, J. Mol. Liq. 248 (2017) 927–942. doi:https://doi.org/10.1016/j.molliq.2017.10.094.

[28]   E.D. Bates, R.D. Mayton, I. Ntai, J.H. Davis, CO2 Capture by a Task-Specific Ionic Liquid, J. Am. Chem. Soc. 124 (2002) 926–927. doi:10.1021/ja017593d.

[29]   P. Hu, R. Zhang, Z. Liu, H. Liu, C. Xu, X. Meng, M. Liang, S. Liang, Absorption Performance and Mechanism of CO2 in Aqueous Solutions of Amine-Based Ionic Liquids, Energy and Fuels. 29 (2015) 6019–6024. doi:10.1021/acs.energyfuels.5b01062.

[30]   Z.-Z. Yang, L.-N. He, S.-Y. Peng, A.-H. Liu, Lewis basic ionic liquids-catalyzed synthesis of 5-aryl-2-oxazolidinones from aziridines and CO2 under solvent-free conditions, Green Chem. 12 (2010) 1850–1854. doi:10.1039/C0GC00286K.

[31]   Y. Zhen-Zhen, H. Liang-Nian, M. Cheng-Xia, C. Sébastien, Lewis Basic Ionic Liquids-Catalyzed Conversion of Carbon Dioxide to Cyclic Carbonates, Adv. Synth. Catal. 352 (2010) 2233–2240. doi:10.1002/adsc.201000239.

[32]   K.E. Gutwoski, E.J. Maginn, Amine functionalized task specific ionic liquids: a mechanistic explanation for the dramatic increase in viscosity upon complexion with CO_2 from molecular simulation, J. Am. Chem. Soc. 130 (2008) 14690–14704.

[33]   K.M. Docherty, C.F. Kulpa, Jr., Toxicity and antimicrobial activity of imidazolium and pyridinium ionic liquids, Green Chem. 7 (2005) 185–189. doi:10.1039/B419172B.

[34]   R.J. Bernot, M.A. Brueseke, M.A. Evans-White, G.A. Lamberti, Acute and chronic toxicity of imidazolium-based ionic liquids on Daphnia magna, Environ. Toxicol. Chem. 24 (2005) 87–92. doi:10.1897/03-635.1.

[35]   K.D. Weaver, H.J. Kim, J. Sun, D.R. MacFarlane, G.D. Elliott, Cyto-toxicity and biocompatibility of a family of choline phosphate ionic liquids designed for pharmaceutical applications, Green Chem. 12 (2010) 507–513. doi:10.1039/B918726J.

[36] W. Gouveia, T.F. Jorge, S. Martins, M. Meireles, M. Carolino, C. Cruz, T. V. Almeida, M.E.M. Araújo, Toxicity of ionic liquids prepared from biomaterials, Chemosphere. 104 (2014) 51–56. doi:10.1016/j.chemosphere.2013.10.055.

[37] M. Petkovic, J.L. Ferguson, H.Q.N. Gunaratne, R. Ferreira, M.C. Leitão, K.R. Seddon, L.P.N. Rebelo, C.S. Pereira, Novel biocompatible cholinium-based ionic liquids—toxicity and biodegradability, Green Chem. 12 (2010) 643–649. doi:10.1039/B922247B.

[38] Y.S. Sistla, A. Khanna, CO2 absorption studies in amino acid-anion based ionic liquids, Chem. Eng. J. 273 (2015) 268–276. doi:10.1016/j.cej.2014.09.043.

[39] B.E. Gurkan, J.C. de la Fuente, E.M. Mindrup, L.E. Ficke, B.F. Goodrich, E.A. Price, W.F. Schneider, J.F. Brennecke, Equimolar CO2 Absorption by Anion-Functionalized Ionic Liquids, J. Am. Chem. Soc. 132 (2010) 2116–2117. doi:10.1021/ja909305t.

[40] Q.-P. Liu, X.-D. Hou, N. Li, M.-H. Zong, Ionic liquids from renewable biomaterials: synthesis, characterization and application in the pretreatment of biomass, Green Chem. 14 (2012) 304–307. doi:10.1039/C2GC16128A.

[41] X. Li, M. Hou, Z. Zhang, B. Han, G. Yang, X. Wang, L. Zou, Absorption of CO2 by ionic liquid/polyethylene glycol mixture and the thermodynamic parameters, Green Chem. 10 (2008) 879. doi:10.1039/b801948g.

[42] S.H. Baharuddin, N.A. Mustahil, A.A. Abdullah, M. Sivapragasam, M. Moniruzzaman, Ecotoxicity study of amino acid ionic liquids towards danio rerio fish: Effect of cations, Procedia Eng. 148 (2016) 401–408. doi:10.1016/j.proeng.2016.06.431.

[43] S. De Santis, G. Masci, F. Casciotta, R. Caminiti, E. Scarpellini, M. Campetella, L. Gontrani, Cholinium-amino acid based ionic liquids: a new method of synthesis and physico-chemical characterization, Phys. Chem. Chem. Phys. 17 (2015) 20687–20698. doi:10.1039/C5CP01612F.

[44] D.-J. Tao, Z. Cheng, F.-F. Chen, Z.-M. Li, N. Hu, X.-S. Chen, Synthesis and Thermophysical Properties of Biocompatible Cholinium-Based Amino Acid Ionic Liquids, (2013). doi:10.1021/je301103d.

[45] S. Yuan, Y. Chen, X. Ji, Z. Yang, X. Lu, Experimental study of CO2absorption in aqueous cholinium-based ionic liquids, Fluid Phase Equilib. 445 (2017) 14–24. doi:10.1016/j.fluid.2017.04.001.

[46] M. Campetella, A. Le Donne, M. Daniele, L. Gontrani, S. Lupi, E. Bodo, F. Leonelli, Hydrogen Bonding Features in Cholinium-Based Protic Ionic Liquids from Molecular Dynamics Simulations, J. Phys. Chem. B. 122 (2018) 2635–2645. doi:10.1021/acs.jpcb.7b12455.

[47] L. Gontrani, Choline-amino acid ionic liquids: past and recent achievements about the structure and properties of these really "green" chemicals, Biophys. Rev. 10 (2018) 873–880. doi:10.1007/s12551-018-0420-9.

[48] J.G. Vitillo, Magnesium-based systems for carbon dioxide capture, storage and recycling: from leaves to synthetic nanostructured materials, RSC Adv. 5 (2015) 36192–36239. doi:10.1039/C5RA02835C.

[49] N.B. Colthup, L.H. Daly, S.E. Wiberley, Introduction to Infrared and Raman Spectroscopy (Third Edition), 3rd ed., Academic Press, San Diego, 1990. doi:10.1016/C2009-0-21628-X.

[50] M.T. Rosado, M.L.T.. Duarte, R. Fausto, Vibrational spectra of acid and alkaline glycine salts, Vib. Spectrosc. 16 (1998) 35–54. doi:10.1016/S0924-2031(97)00050-7.

[51] A.W. Herlinger, T.V. Long, Laser-Raman and Infrared Spectra of Amino Acids and Their Metal Complexes. III. Proline and Bisprolinato Complexes, J. Am. Chem. Soc. 92 (1970)

6481–6486.

[52]   J. van Holst, G.F. Versteeg, D.W.F. Brilman, J.A. Hogendoorn, Kinetic study of CO2 with various amino acid salts in aqueous solution, Chem. Eng. Sci. 64 (2009) 59–68. doi:10.1016/j.ces.2008.09.015.

[53]   R.K. Khanna, M.H. Moore, Carbamic acid: molecular structure and IR spectra., Spectrochim. Acta. A. Mol. Biomol. Spectrosc. 55A (1999) 961–967. doi:10.1016/S1386-1425(98)00228-5.

[54]   M.L. Pinto, L. Mafra, J.M. Guil, J. Pires, J. Rocha, Adsorption and activation of CO2 by amine-modified nanoporous materials studied by solid-state NMR and 13CO2 adsorption, Chem. Mater. 23 (2011) 1387–1395. doi:10.1021/cm1029563.

[55]   C. Knöfel, C. Martin, V. Hornebecq, P.L. Llewellyn, Study of carbon dioxide adsorption on mesoporous aminopropylsilane- functionalized silica and titania combining microcalorimetry and in situ infrared spectroscopy, J. Phys. Chem. C. 113 (2009) 21726–21734. doi:10.1021/jp907054h.

[56]   G. Gatti, D. Costenaro, C. Vittoni, G. Paul, V. Crocellà, E. Mangano, S. Brandani, S. Bordiga, M. Cossi, L. Marchese, C. Bisio, CO2adsorption on different organo-modified SBA-15 silicas: A multidisciplinary study on the effects of basic surface groups, Phys. Chem. Chem. Phys. 19 (2017) 14114–14128. doi:10.1039/c6cp08048k.

[57]   D.L.B. Robert M. Silverstein, Francis X. Webster, David J. Kiemle, Textbook Spectrometric Identification of Organic Compounds, 8th ed., 2015.

[58]   V. Crocellà, T. Tabanelli, J.G. Vitillo, D. Costenaro, C. Bisio, F. Cavani, S. Bordiga, Applied Catalysis B : Environmental A multi-technique approach to disclose the reaction mechanism of dimethyl carbonate synthesis over amino-modified SBA-15 catalysts, "Applied Catal. B, Environ. 211 (2017) 323–336. doi:10.1016/j.apcatb.2017.04.013.

[59]   M.W. Hahn, M. Steib, A. Jentys, J.A. Lercher, Mechanism and Kinetics of CO 2 Adsorption on Surface Bonded Amines, J. Phys. Chem. C. 119 (2015) 4126–4135. doi:10.1021/jp512001t.

[60]   J.B. Bossa, F. Borget, F. Duvernay, P. Theulé, T. Chiavassa, H. Hill, Formation of neutral methylcarbamic acid (CH3NHCOOH) and methylammonium methylcarbamate [CH3NH3+][CH3NHCO2-] at low temperature, J. Phys. Chem. A. 112 (2008) 5113–5120. doi:10.1021/jp800723c.

[61]   A. Danon, P.C. Stair, E. Weitz, FTIR Study of CO 2 Adsorption on Amine-Grafted SBA-15: Elucidation of Adsorbed Species, J. Phys. Chem. C. 115 (2011) 11540–11549. doi:10.1021/jp200914v.

[62]   X. Wang, V. Schwartz, J.C. Clark, X. Ma, S.H. Overbury, X. Xu, C. Song, Infrared Study of CO 2 Sorption over "Molecular Basket" Sorbent Consisting of Polyethylenimine-Modified Mesoporous Molecular Sieve, J. Phys. Chem. C. 113 (2009) 7260–7268. doi:10.1021/jp809946y.